Chapter 3

Bioconvective stagnation-point flow due to induced magnetic field *

3.1 Introduction

The nanofluid studies involving microorganisms is an advancing field that has intrigued researchers due to its relevance in antibiotics, biofuel, toxin removal, targeted drug delivery and food digestion. The magnetic field represents an important characteristic of hydromagnetic problems. However, studies incorporating induced magnetic field (the additional magnetic field that gets induced on electrically conducting fluid when encountered with an external magnetic field caused due to the impact of a larger magnetic Reynolds number) effects are limited in number. For its applications in biomedical imaging, hyperthermia, targeted drug delivery, and cancer therapy, the bioconvective stagnation point flow involving carbon nanotubes along a lengthening sheet subject to induced magnetic field and multiple stratification effects is investigated. Additionally, chemical reaction and viscous dissipation effects are also heeded. Relevant similarity formulas are effectuated in converting the modeled equations into a first-order system of ODEs and are further treated in MATLAB using *ode45* and Newton Raphson method. Illustrations on the consequence of effectual parameters on the physical quantities and the flow profiles are achieved with the aid of graphs.

*Published in: ZAMM - Journal of Applied Mathematics and Mechanics (Wiley), 2021; 101(11); e202000375.

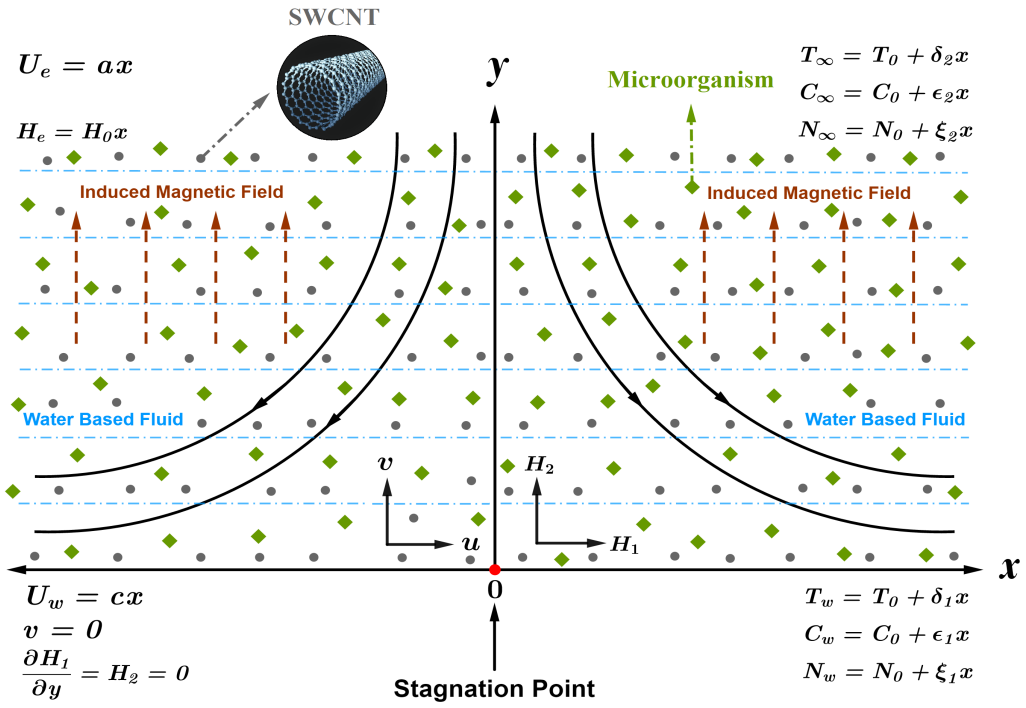

Figure 3.1: Geometrical Frame

3.2 Mathematical Frame

Two-dimensional steady incompressible bioconvective stagnation point flow over a linearly elongating sheet (see Figure 3.1) is considered under the ensuing assumptions:

- The expanding sheet is positioned along x axis and water-based SWCNT nanofluid (containing microorganisms) occupies the region $y > 0$.
- $U_w(x) = cx$ and $U_e(x) = ax$ correspond to the velocity of the lengthening sheet and the free stream, respectively.
- Induced magnetic field vector, $H = (H_1, H_2)$ is considered with H_1 & H_2 being the magnetic integrants along x and y direction, respectively.
- Chemical reaction and viscous dissipation effects are incorporated.
- Motile density, thermal, and solutal stratification effects are also considered.

Following the aforementioned assumptions, the governing equations are written as (see Alsaedi et al., 2017; Z. Iqbal, Azhar, & Maraj, 2017):

$$\frac{\partial u}{\partial x}+\frac{\partial v}{\partial y}=0 \tag{3.2.1}$$

$$\frac{\partial H_1}{\partial x}+\frac{\partial H_2}{\partial y}=0 \tag{3.2.2}$$

$$u\frac{\partial u}{\partial x}+v\frac{\partial u}{\partial y}-\frac{\mu_e}{4\pi\rho_{nf}}\left(H_1\frac{\partial H_1}{\partial x}+H_2\frac{\partial H_1}{\partial y}\right)=U_e\frac{dU_e}{dx} - \frac{\mu_e H_e}{4\pi\rho_{nf}}\frac{dH_e}{dx}+\left(\frac{\mu_{nf}}{\rho_{nf}}\right)\frac{\partial^2 u}{\partial y^2} \tag{3.2.3}$$

$$u\frac{\partial H_1}{\partial x}+v\frac{\partial H_1}{\partial y}-H_1\frac{\partial u}{\partial x}-H_2\frac{\partial u}{\partial y}=\alpha_m\frac{\partial^2 H_1}{\partial y^2} \tag{3.2.4}$$

$$u\frac{\partial T}{\partial x}+v\frac{\partial T}{\partial y}=\alpha_{nf}\frac{\partial^2 T}{\partial y^2}+\frac{\mu_{nf}}{(\rho C_p)_{nf}}\left(\frac{\partial u}{\partial y}\right)^2 \tag{3.2.5}$$

$$u\frac{\partial C}{\partial x}+v\frac{\partial C}{\partial y}=D_B\frac{\partial^2 C}{\partial y^2}-k_r\left(C-C_\infty\right) \tag{3.2.6}$$

$$u\frac{\partial N}{\partial x}+v\frac{\partial N}{\partial y}+\frac{bW_c}{C_w-C_0}\left(\frac{\partial}{\partial y}\left(N\frac{\partial C}{\partial y}\right)\right)=D_m\frac{\partial^2 N}{\partial y^2} \tag{3.2.7}$$

subject to the boundary conditions (see Alsaedi et al., 2017; Z. Iqbal, Azhar, & Maraj, 2017):

$$\begin{gathered} u=U_w(x)=cx,\ v=0,\ \tfrac{\partial H_1}{\partial y}=H_2=0,\ T=T_w=T_0+\delta_1 x, \\ C=C_w=C_0+\epsilon_1 x,\ N=N_w=N_0+\xi_1 x \qquad \text{at } y=0 \end{gathered}$$

$$\begin{gathered} u\to U_e(x)=ax,\ H_1\to H_e(x)=H_0 x,\ T\to T_\infty=T_0+\delta_2 x, \\ C\to C_\infty=C_0+\epsilon_2 x,\ N\to N_\infty=N_0+\xi_2 x \qquad \text{as } y\to\infty \end{gathered}$$

where $\alpha_m=\dfrac{1}{4\pi\mu_e\sigma_{nf}}$ represents the magnetic diffusivity.

Consider the following similarity transformations (see Alsaedi et al., 2017; Z. Iqbal, Azhar, & Maraj, 2017):

$$u=cxf\,'(\zeta),\ v=-\sqrt{c\vartheta_f}f(\zeta),\ H_1=H_0xg\,'(\zeta),\ \zeta=y\sqrt{\frac{c}{\vartheta_f}},\ H_2=-H_0\sqrt{\frac{\vartheta_f}{c}}g(\zeta),$$

$$\theta(\zeta)=\frac{T-T_\infty}{T_w-T_0},\ \psi(\zeta)=\frac{C-C_\infty}{C_w-C_0},\ \chi(\zeta)=\frac{N-N_\infty}{N_w-N_0}$$

Employing the similarity transformations into Equations (3.2.1) – (3.2.7), we get:

$$f\,''' - A_1\,A_2\left\{(\,f\,')^2 - f\,f\,'' - \frac{\beta}{A_2}\left\{(\,g\,')^2 - g\,g\,'' - 1\right\} - A^2\right\} = 0 \tag{3.2.8}$$

$$g\,''' - \frac{A_5}{\lambda}\,\{\,g\,f\,'' - f\,g\,''\,\} = 0 \tag{3.2.9}$$

$$\theta\,'' + \frac{A_3\,Pr}{A_4}\,f\,\theta\,' + \frac{Ec\,Pr}{A_1\,A_4}\,(\,f\,'')^2 = 0 \tag{3.2.10}$$

$$\psi\,'' + Le\,f\,\psi\,' - Kr\,Le\,\psi = 0 \tag{3.2.11}$$

$$\chi\,'' + Lb\,f\,\chi\,' - Pe\,\{\,(\,\chi + \Omega\,)\,\psi\,'' + \chi\,'\,\psi\,'\,\} = 0 \tag{3.2.12}$$

subject to the boundary conditions

$$f(\zeta) = 0, \quad f\,'(\zeta) = 1, \quad g(\zeta) = 0, \quad g\,''(\zeta) = 0, \quad \theta(\zeta) = 1 - s_1,$$
$$\psi(\zeta) = 1 - s_2, \quad \chi(\zeta) = 1 - s_3 \quad \text{when } \zeta = 0$$

$$f'(\zeta) \to A, \quad g\,'(\zeta) \to 1, \quad \theta(\zeta) \to 0,$$
$$\psi(\zeta) \to 0, \quad \chi(\zeta) \to 0 \quad \text{as } \zeta \to \infty$$

where the dimensionless parameters are given in appendix I.

The nanofluid models incorporated are (see Z. Iqbal, Azhar, & Maraj, 2017; Sreedevi & Reddy, 2019):

Effective Dynamic Viscosity : $\dfrac{\mu_{nf}}{\mu_f} = \dfrac{1}{(1-\phi)^{2.5}} = \dfrac{1}{A_1}$

Effective Density : $\dfrac{\rho_{nf}}{\rho_f} = (1-\phi) + \phi\left(\dfrac{\rho_{SWCNT}}{\rho_f}\right) = A_2$

Effective Specific Heat : $\dfrac{(\rho C_p)_{nf}}{(\rho C_p)_f} = (1-\phi) + \phi\left(\dfrac{(\rho C_p)_{SWCNT}}{(\rho C_p)_f}\right) = A_3$

Effective Thermal Conductivity : $\dfrac{k_{nf}}{k_f} = \dfrac{(1-\phi) + 2\phi\,\frac{k_{SWCNT}}{k_{SWCNT}-k_f}\,ln\left(\frac{k_{SWCNT}+k_f}{2k_f}\right)}{(1-\phi) + 2\phi\,\frac{k_f}{k_{SWCNT}-k_f}\,ln\left(\frac{k_{SWCNT}+k_f}{2k_f}\right)} = A_4$

$$\text{Effective Electrical Conductivity} \quad : \quad \frac{\sigma_{nf}}{\sigma_f} = 1 + \frac{3\left(\frac{\sigma_{SWCNT}}{\sigma_f} - 1\right)\phi}{\left(\frac{\sigma_{SWCNT}}{\sigma_f} + 2\right) - \left(\frac{\sigma_{SWCNT}}{\sigma_f} - 1\right)\phi} = A_5$$

The physical quantities are given by (see Alsaedi et al., 2017; Z. Iqbal, Azhar, & Maraj, 2017):

$$\text{Local drag coefficient} \quad : \quad Cf_x = \frac{\tau_\omega}{\rho_f \ (U_w)^2} = \frac{\mu_{nf} \ \frac{\partial u}{\partial y}\Big|_{y=0}}{\rho_f \ (U_w)^2}$$

$$\Rightarrow \ Cf_x \ Re_x^{1/2} = \frac{f\,''(0)}{A_1}$$

$$\text{Local Nusselt number} \quad : \quad Nu_x = \frac{x \ q_\omega}{k_f \ (T_w - T_0)} = \frac{-x \ k_{nf} \ \frac{\partial T}{\partial y}\Big|_{y=0}}{k_f \ (T_w - T_0)}$$

$$\Rightarrow \ Nu_x \ Re_x^{-\ 1/2} = -A_4 \ \theta\,'(0)$$

$$\text{Local Sherwood number} \quad : \quad Sh_x = \frac{x \ q_m}{D_B \ (C_w - C_0)} = \frac{-x \ D_B \ \frac{\partial C}{\partial y}\Big|_{y=0}}{D_B \ (C_w - C_0)}$$

$$\Rightarrow \ Sh_x \ Re_x^{-\ 1/2} = -\ \psi\,'(0)$$

$$\text{Local motile density number} \quad : \quad Nn_x = \frac{x \ q_n}{D_m \ (N_w - N_0)} = \frac{-x \ D_m \ \frac{\partial N}{\partial y}\Big|_{y=0}}{D_m \ (N_w - N_0)}$$

$$\Rightarrow \ Nn_x \ Re_x^{-\ 1/2} = -\ \chi\,'(0)$$

where $Re_x = \frac{xU_w}{\vartheta_f}$ is the local Reynold's number.

3.3 Numerical Frame & Validation

Equations (3.2.8) - (3.2.12) together with the boundary conditions are numerically resolved in MATLAB employing *ode45* (for solving) and Newton Raphson method (for shooting). This is accomplished by initially assuming:

$$\Gamma_1 = f, \quad \Gamma_2 = f\,', \quad \Gamma_3 = f\,'', \quad \Gamma_3{}' = f\,''', \quad \Gamma_4 = g, \quad \Gamma_5 = g\,',$$
$$\Gamma_6 = g\,'', \quad \Gamma_6{}' = g\,''', \quad \Gamma_7 = \theta, \quad \Gamma_8 = \theta\,', \quad \Gamma_8{}' = \theta\,'', \quad \Gamma_9 = \psi,$$
$$\Gamma_{10} = \psi\,', \quad \Gamma_{10}{}' = \psi\,'', \quad \Gamma_{11} = \chi, \quad \Gamma_{12} = \chi\,', \quad \Gamma_{12}{}' = \chi\,''$$

The reduced system of the first-order ODE is given by:

$$\Gamma_1{}' = \Gamma_2 \ , \ \Gamma_2{}' = \Gamma_3 \ ,$$

$$\Gamma_3{}' = A_1 \ A_2 \ \left\{ \ (\Gamma_2)^2 - \Gamma_1 \ \Gamma_3 - \frac{\beta}{A_2} \ \left\{ (\Gamma_5)^2 - \Gamma_4 \ \Gamma_6 - 1 \right\} - A^2 \ \right\} \ ,$$

$$\Gamma_4{}' = \Gamma_5 \ , \ \Gamma_5{}' = \Gamma_6 \ ,$$

$$\Gamma_6{}' = \frac{A_5}{\lambda} \ \{ \ \Gamma_4 \ \Gamma_3 - \Gamma_1 \ \Gamma_6 \ \} \ ,$$

$$\Gamma_7{}' = \Gamma_8 \ , \ \Gamma_8{}' = - \left\{ \frac{A_3 \ Pr}{A_4} \ \Gamma_1 \ \Gamma_8 + \frac{Ec \ Pr}{A_1 \ A_4} \ (\Gamma_3)^2 \right\} \ ,$$

$$\Gamma_9{}' = \Gamma_{10} \ , \ \Gamma_{10}{}' = Kr \ Le \ \Gamma_9 - Le \ \Gamma_1 \ \Gamma_{10} \ ,$$

$$\Gamma_{11}{}' = \Gamma_{12} \ \ , \ \Gamma_{12}{}' = Pe \ \left\{ \ (\Gamma_{11} + \Omega) \ \ \Gamma_{10}{}' + \Gamma_{12} \ \Gamma_{10} \ \right\} - Lb \ \Gamma_1 \ \Gamma_{12} \ .$$

with

$$\begin{gathered} \Gamma_1(0) = 0, \quad \Gamma_2(0) = 1, \quad \Gamma_3(0) = \Lambda_1, \quad \Gamma_4(0) = 0, \\ \Gamma_5(0) = \Lambda_2, \quad \Gamma_6(0) = 0, \quad \Gamma_7(0) = 1 - s_1, \quad \Gamma_8(0) = \Lambda_3, \\ \Gamma_9(0) = 1 - s_2, \quad \Gamma_{10}(0) = \Lambda_4, \quad \Gamma_{11}(0) = 1 - s_3, \quad \Gamma_{12}(0) = \Lambda_5 \end{gathered}$$

where Λ_1 , Λ_2 , Λ_3 , Λ_4 & Λ_5 are estimated by employing the Newton Raphson method with a befitting initial guess.

The above set of equations are then numerically resolved utilizing *ODE45*, a built-in MATLAB function, with an absolute error tolerance of 10^{-6}. *ODE45* employs a fourth-order Runge-Kutta method with a self-adaptive step size for effective computation. The veracity of the code and the validation of this research work have been adjudged through a restrictive comparison of the present work with prior published works of Hayat et al., 2015, 2016; Iqbal, Azhar, et al., 2017 (showcased in Table 3.1 & 3.2).

3.4 Results & Discussion

The consequence of influential parameters on microbial concentration ($\chi(\zeta)$), velocity ($f'(\zeta)$), concentration ($\psi(\zeta)$), temperature ($\theta(\zeta)$) and induced magnetic field ($g'(\zeta)$) profiles are illustrated via Figures 3.2 - 3.15. Changes in the aforementioned profiles due to stretching parameter (A) are graphed in Figures 3.2, 3.4, 3.7, 3.11

Table 3.1: Comparison of drag coefficient $\left(Cf_x Re_x^{1/2}\right)$ for different A values between the present study and the works of Iqbal, Azhar, et al., 2017 and Hayat et al., 2015, 2016 when $\phi = \beta = 0$

A	$\boldsymbol{Cf_x Re_x^{1/2}}$			
	Iqbal et al., 2017	**Hayat et al., 2015**	**Hayat et al., 2016**	**Present study**
0.1	-0.969386	-0.96939	-0.96937	-0.9693860
0.2	-0.918107	-0.91811	-0.91813	-0.9181071
0.5	-0.667263	-0.66726	-0.66723	-0.6672637
0.7	-0.433475	-0.43346	-0.43345	-0.4334755
0.8	-0.299388	-0.29929	-0.29921	-0.2993888
0.9	-0.154716	-0.15458	-0.1545471	-0.1547167
1	0	0	0	0

Table 3.2: Comparison of $Nu_x Re_x^{-1/2}$ and $-Cf_x Re_x^{1/2}$ for differing ϕ, β, λ values between the present study and (Iqbal, Azhar, et al., 2017)

$\boldsymbol{\phi}$	$\boldsymbol{\beta}$	$\boldsymbol{\lambda}$	$\boldsymbol{-Cf_x Re_x^{1/2}}$		$\boldsymbol{Nu_x Re_x^{-1/2}}$	
			Iqbal et al., 2017	**Present study**	**Iqbal et al., 2017**	**Present study**
0.1	0	1	0.8201	0.82011	2.9371	2.93709
0.2	0	1	1.0139	1.01386	3.7139	3.71387
0	0	1	0.6673	0.66726	1.8581	1.85807
0	0.1	1	0.5759	0.57595	1.8771	1.8771
0	0.2	5	0.5129	0.51293	1.8909	1.89091
0	0.2	10	0.5651	0.56507	1.8802	1.88018

Table 3.3: Thermophysical properties of water and SWCNT

Property	**Water (base fluid)**	**SWCNT (nanoparticle)**
$\boldsymbol{\rho}$	997	2600
$\boldsymbol{C_p}$	4179	425
$\boldsymbol{k}$	0.613	6600
$\boldsymbol{\sigma}$	0.05	10^6

& 3.14. It is perceived that augmenting A values produces a constructive effect on $f'(\zeta)$ and destructive effect on $g'(\zeta)$, $\theta(\zeta)$, $\psi(\zeta)$ & $\chi(\zeta)$. Simultaneous effects of parameters on physical quantities are depicted in Figures 3.16 - 3.20. Studies have been carried out for $A = 0.5$ & $A = 1.5$ with Prandtl number(Pr) and infinity fixed at 6.2 and 6, respectively. Thermophysical properties of the conventional fluid (water) and SWCNT (nanofluid) are showcased in Table 3.3.

Figure 3.3 bespeaks the deviations in $f'(\zeta)$ with respect to β (magnetic parameter). It is noted that $f'(\zeta)$ increases for augmenting β values when $A = 0.5$ and a reversed behaviour is observed for $f'(\zeta)$ when $A = 1.5$. Figure 3.5 depicts the influence of β on $g'(\zeta)$. An elevation in $g'(\zeta)$ for $A = 0.5$ and a demotion when $A = 1.5$ are observed for elevating β values. Figure 3.6 explains the mixed effect of λ (reciprocal of magnetic Prandtl number) on $g'(\zeta)$. Initially, elevating λ values decays $g'(\zeta)$ and afterwards, a reversed trend is observed when $A = 0.5$. A similar but inversed impact is perceived when $A = 1.5$.

Variation in $\theta(\zeta)$ due to Eckert number (Ec) is elucidated in Figure 3.8 and it is noted that augmenting Ec numerals fuels an increase in $\theta(\zeta)$. Physically, this result can be associated with the generation of friction forces between the fluid particles which increases the nanomaterial temperature. The ascending nature of $\theta(\zeta)$ with ϕ (volume fraction of nanoparticle) is illustrated in Figure 3.9. This increase in temperature can be physically related to the improvement in the thermal conductivity of the nanoliquid caused by larger nanoparticle occupancy. Figure 3.10 explains the consequence of s_1 (thermal stratification parameter) on $\theta(\zeta)$. A decreasing behaviour is noticed and this is due to the waning temperature differences. Physically, the decrease in the nanofluid temperature is due to the drop in the temperature difference between the surface and away from the surface caused by an increase in s_1.

With a rise in the magnitude of Kr (chemical reaction parameter), depletion in $\psi(\zeta)$ is observed which has been plotted in Figure 3.12. The physical explanation being that the increased chemical reaction eats up the nanoparticle which induces shrinkage in the concentration profile. Figure 3.13 reveals the change in $\psi(\zeta)$ with ascending s_2 (solutal stratification parameter). An increase in s_2 prompts a decrease in the volumetric fraction which sources a fall in $\psi(\zeta)$. Physically, an increase in s_2 descends the concentration profile due to the decrease in the volumetric fraction

between the surface and reference nanoparticles. Figure 3.15 describes the negative influence of s_3 (motile density stratification parameter) on $\chi(\zeta)$. This is because an augmentation in s_3 decreases the concentration difference of microorganisms between the surface and away from the surface and hence the microbial concentration decreases.

One can interpret from Figure 3.16 that $Cf_x Re_x^{1/2}$ increases with β and decreases with ϕ when $A = 0.5$. For $A = 1.5$, $Cf_x Re_x^{1/2}$ improves with ϕ and deteriorates with β. Physically, stretching parameter corresponds to the ratio of free stream velocity to the stretching sheet velocity. For $A > 1$, there is an increase in the straining motion near the stagnation region that results in the acceleration of free stream. However, for $A < 1$, the flow has an inverted boundary layer structure. Hence, the results of skin friction are negative for $A = 0.5$. From Figures 3.17 & 3.18, it is clear that $Nu_x Re_x^{-1/2}$ (both cases) ascends with ϕ and descends with Ec & s_1. Figure 3.19 demonstrates the escalating and declining behaviour of Kr & s_2 on $Sh_x Re_x^{-1/2}$ (both cases), respectively. Figure 3.20 depicts that Kr causes a rise in $Nn_x Re_x^{-1/2}$ (both cases) whereas a fall in $Nn_x Re_x^{-1/2}$ (both cases) is observed due to s_3.

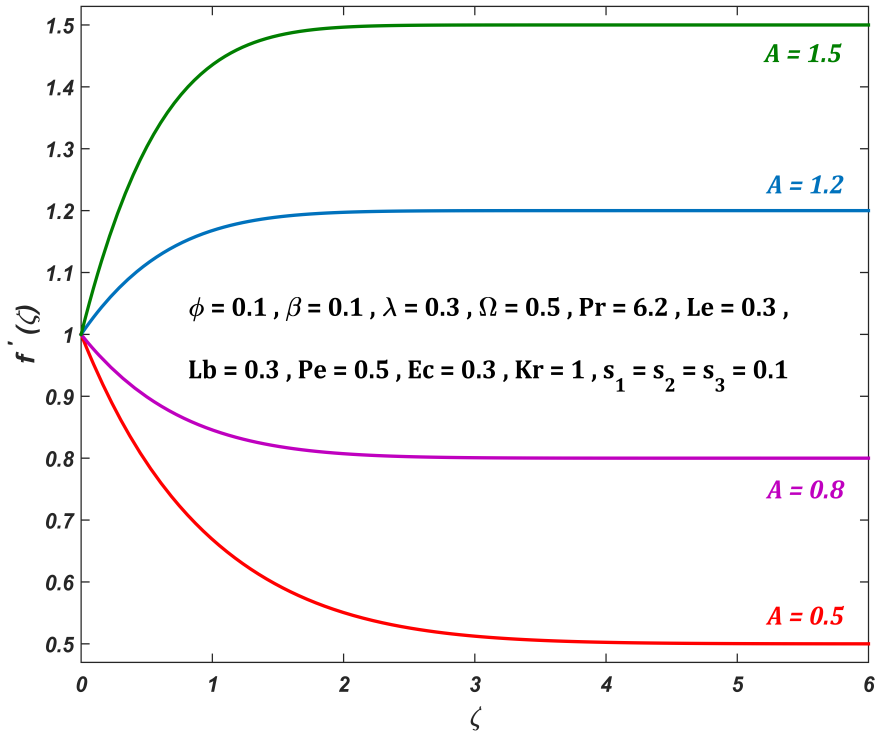

Figure 3.2: $f'(\zeta)$ for differing A values

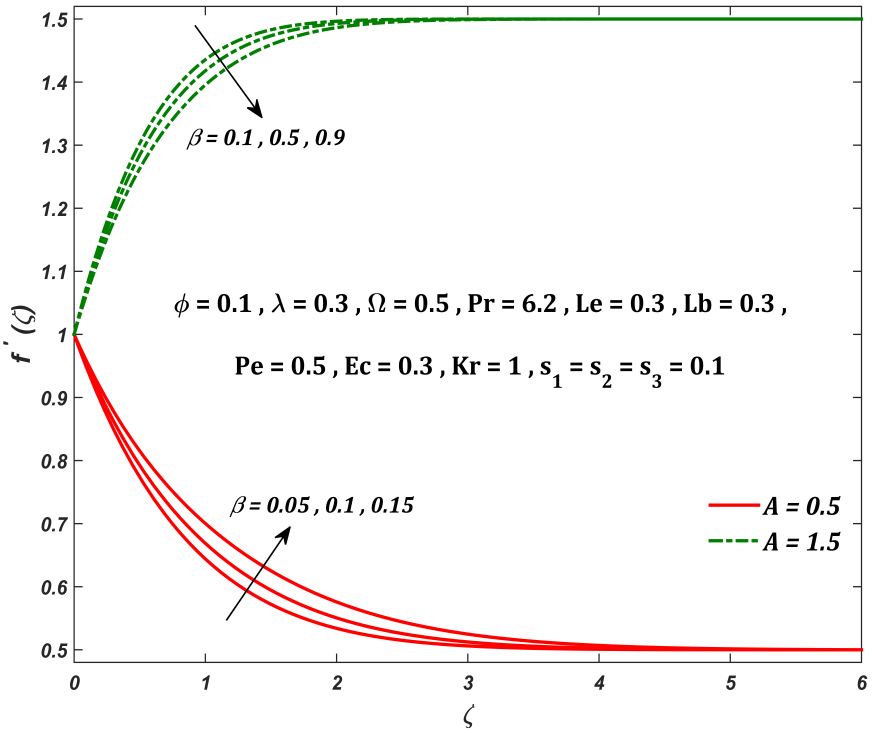

Figure 3.3: $f'(\zeta)$ for differing β values

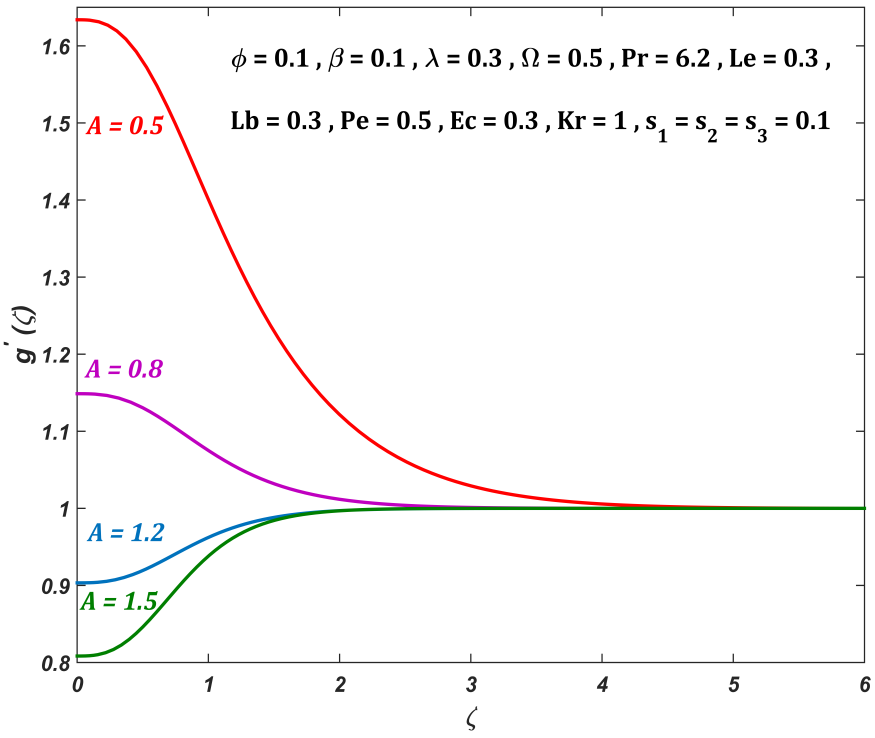

Figure 3.4: $g'(\zeta)$ for differing A values

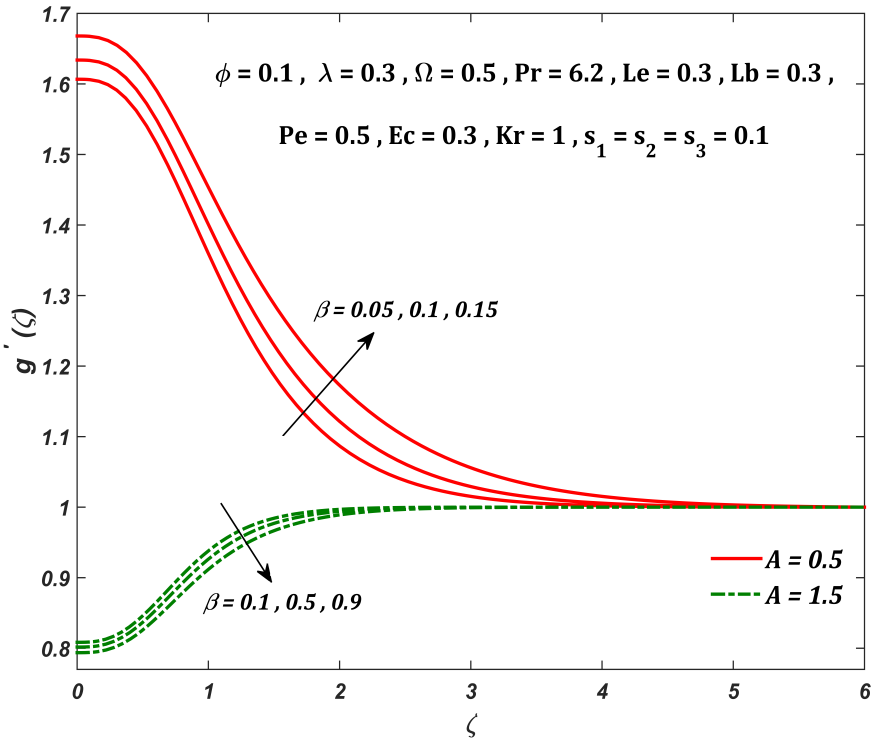

Figure 3.5: $g'(\zeta)$ for differing β values

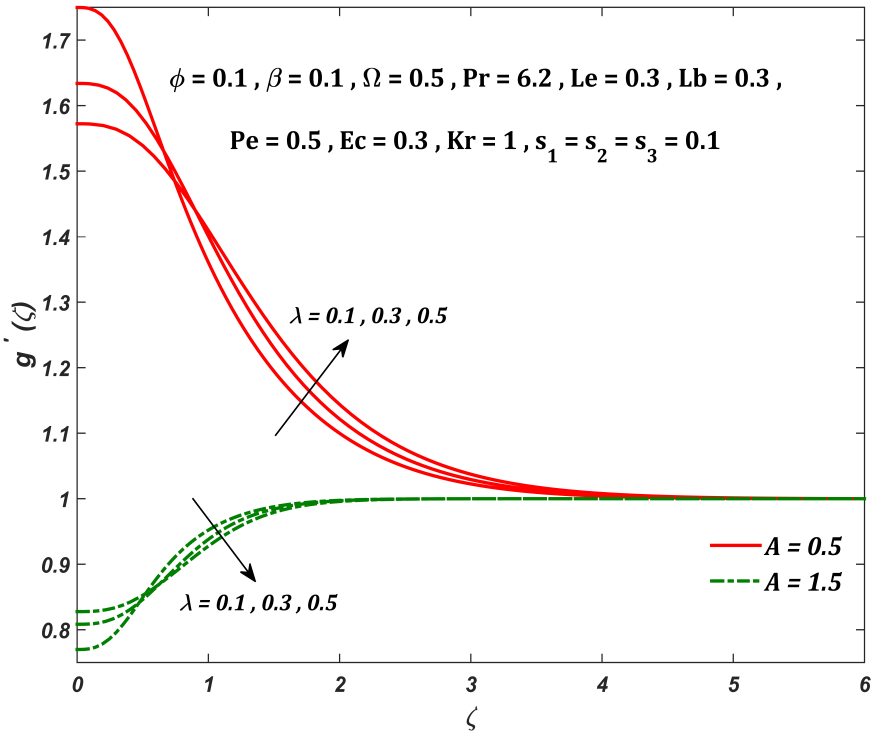

Figure 3.6: $g'(\zeta)$ for differing λ values

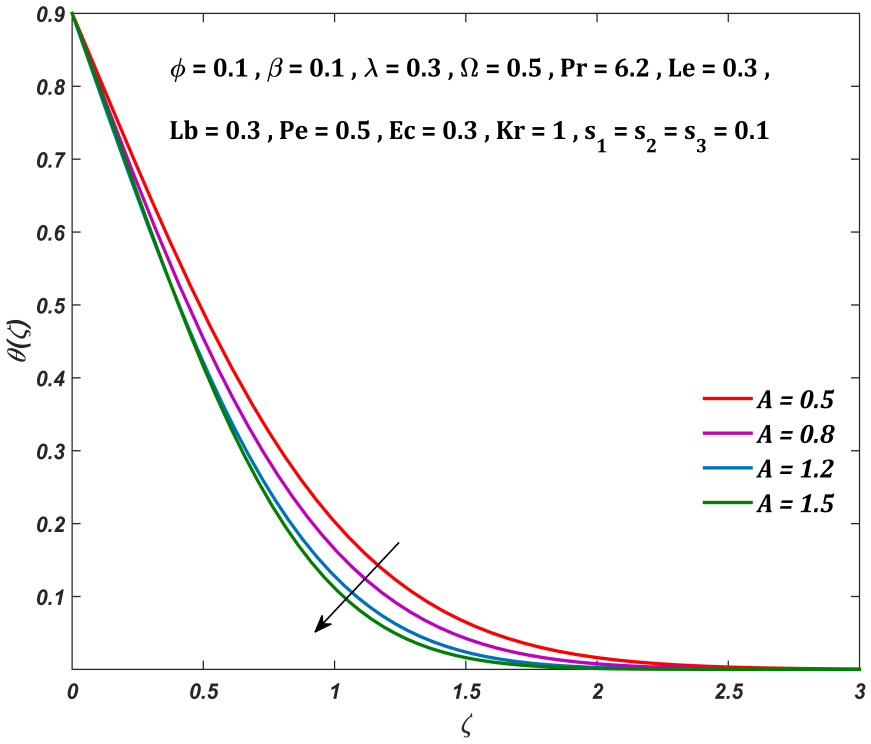

Figure 3.7: $\theta\,(\zeta)$ for differing A values

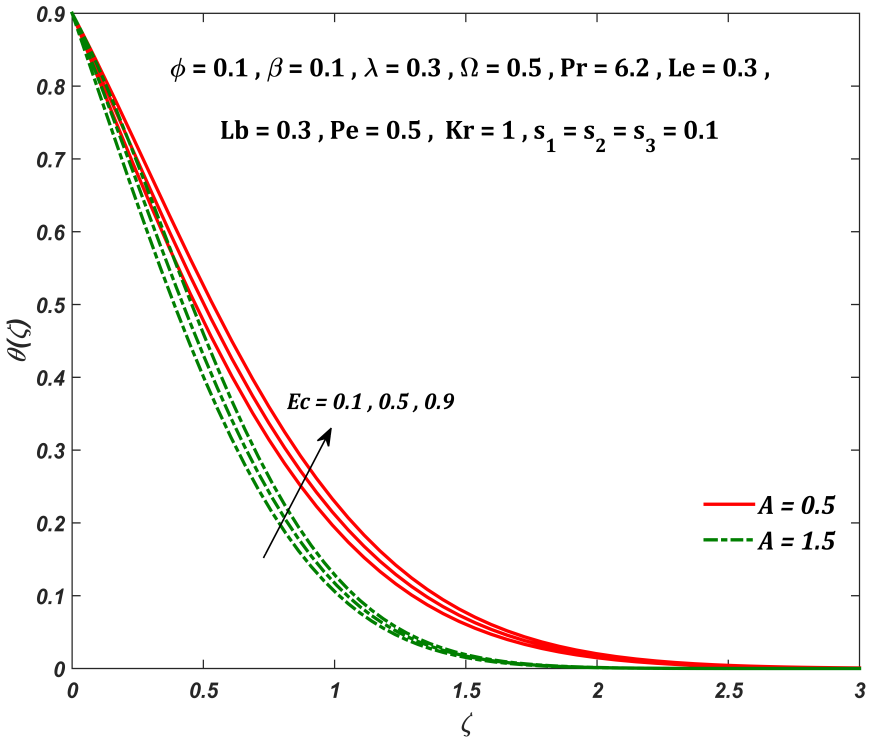

Figure 3.8: $\theta\,(\zeta)$ for differing Ec values

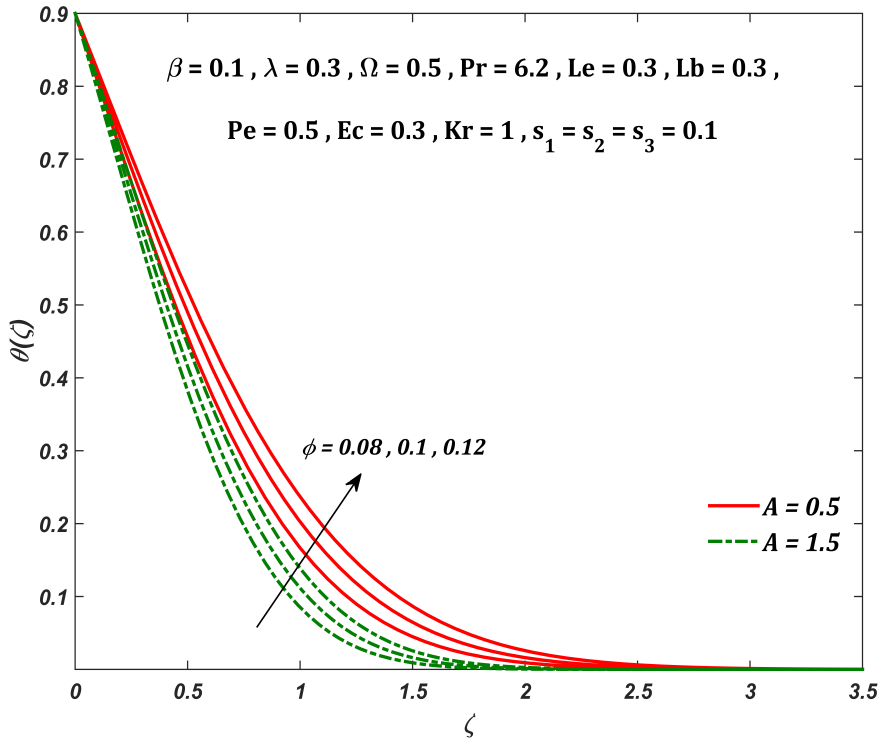

Figure 3.9: $\theta(\zeta)$ for differing ϕ values

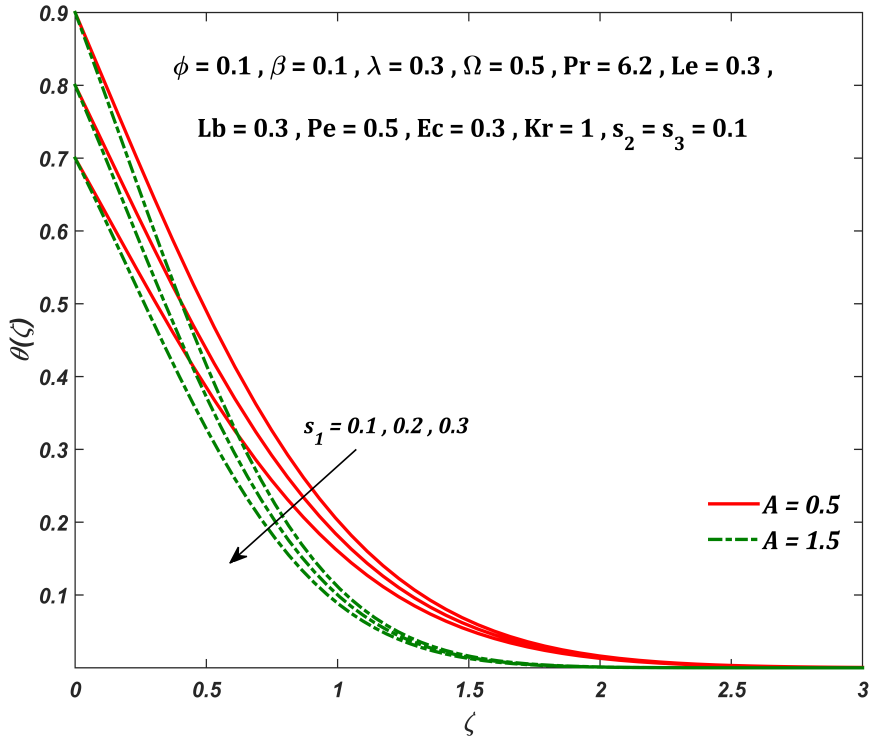

Figure 3.10: $\theta(\zeta)$ for differing s_1 values

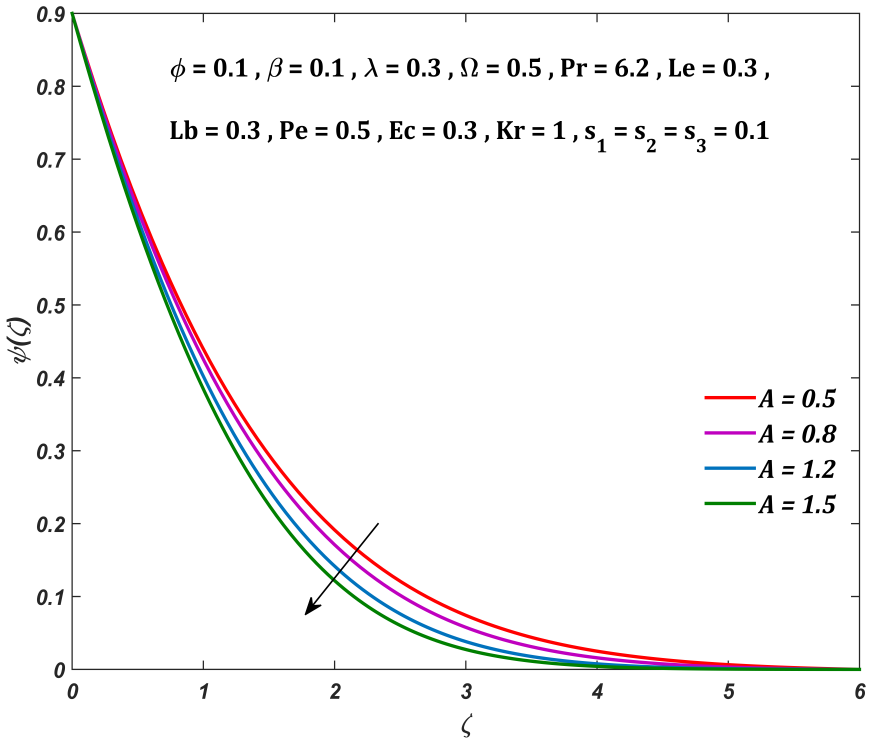

Figure 3.11: $\psi(\zeta)$ for differing A values

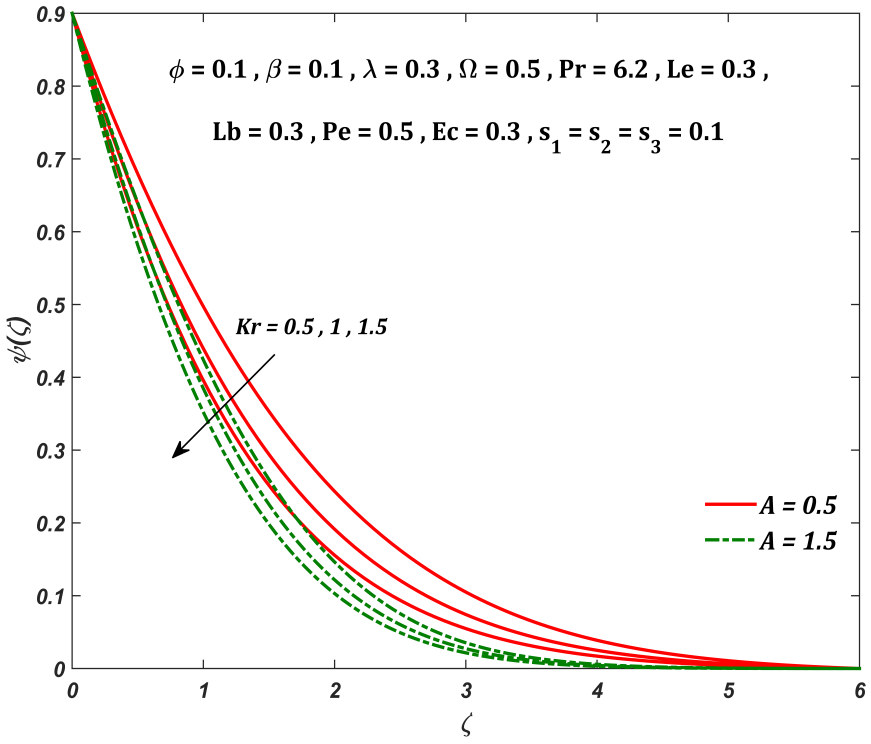

Figure 3.12: $\psi(\zeta)$ for differing Kr values

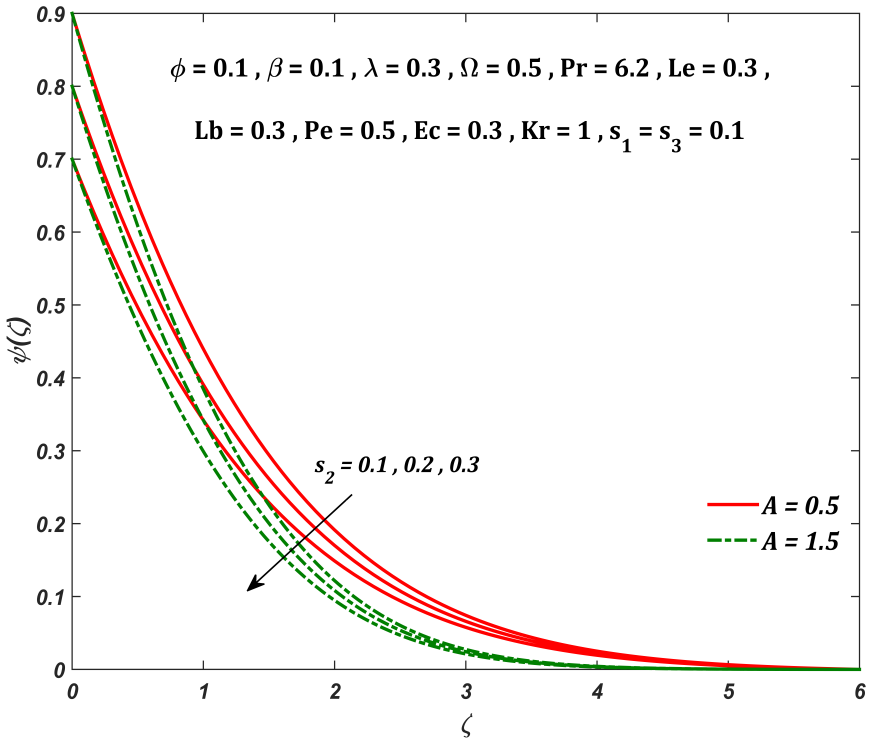

Figure 3.13: $\psi\,(\zeta)$ for differing s_2 values

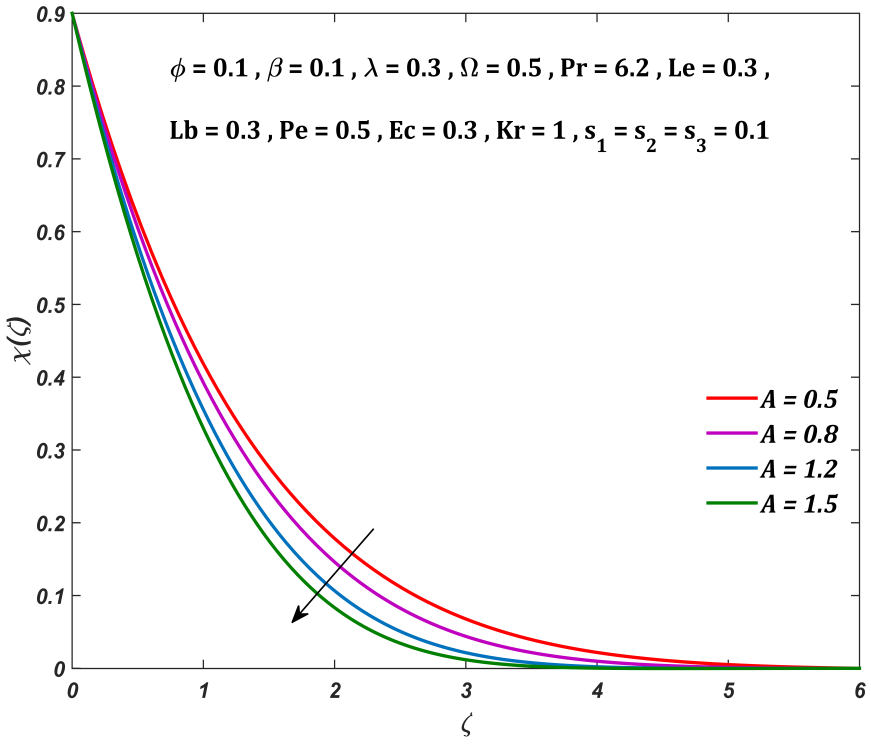

Figure 3.14: $\chi\,(\zeta)$ for differing A values

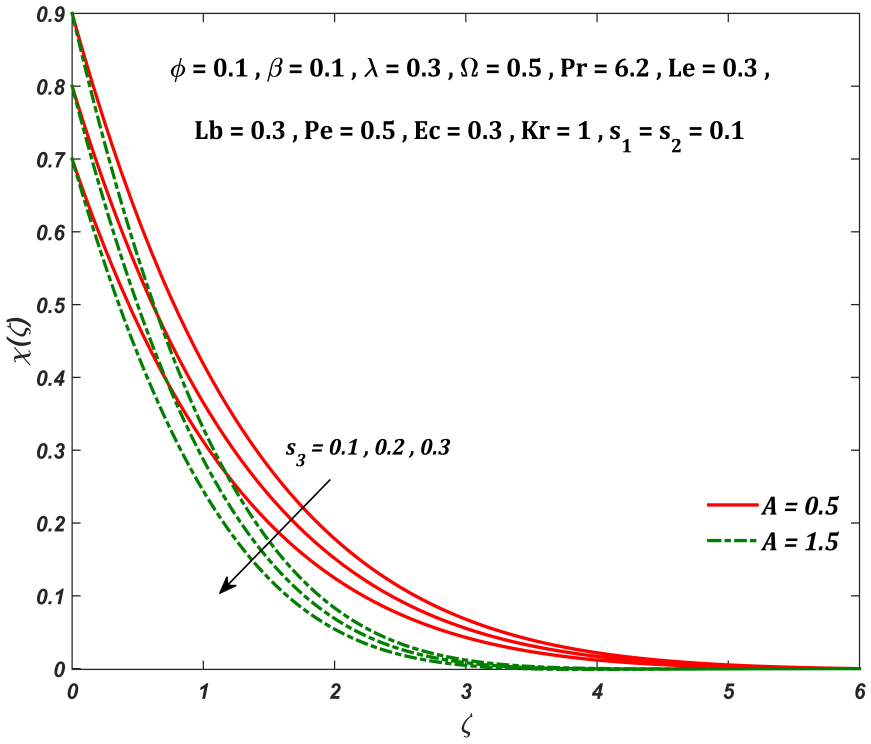

Figure 3.15: $\chi\,(\zeta)$ for differing s_3 values

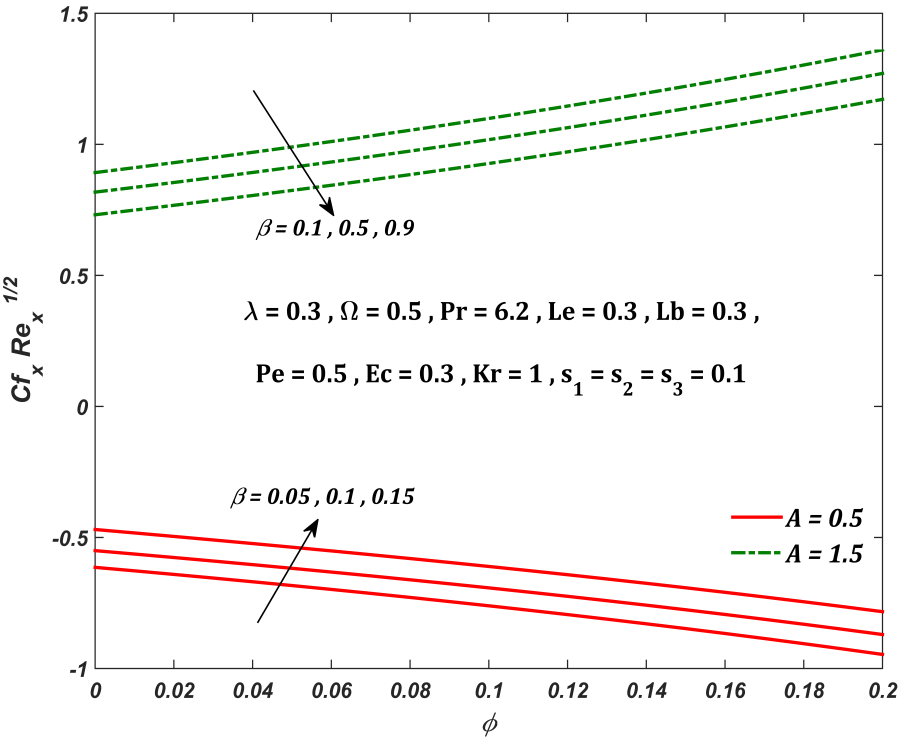

Figure 3.16: Parallel effect of ϕ & β on $Cf_x Re_x^{1/2}$

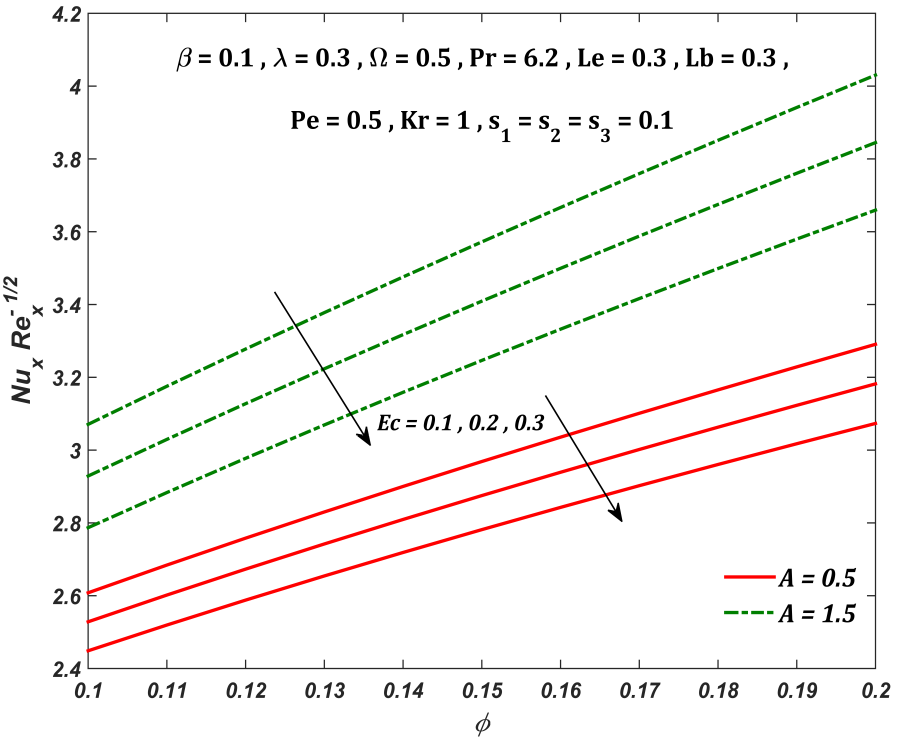

Figure 3.17: Parallel effect of ϕ & Ec on $Nu_x Re_x^{-1/2}$

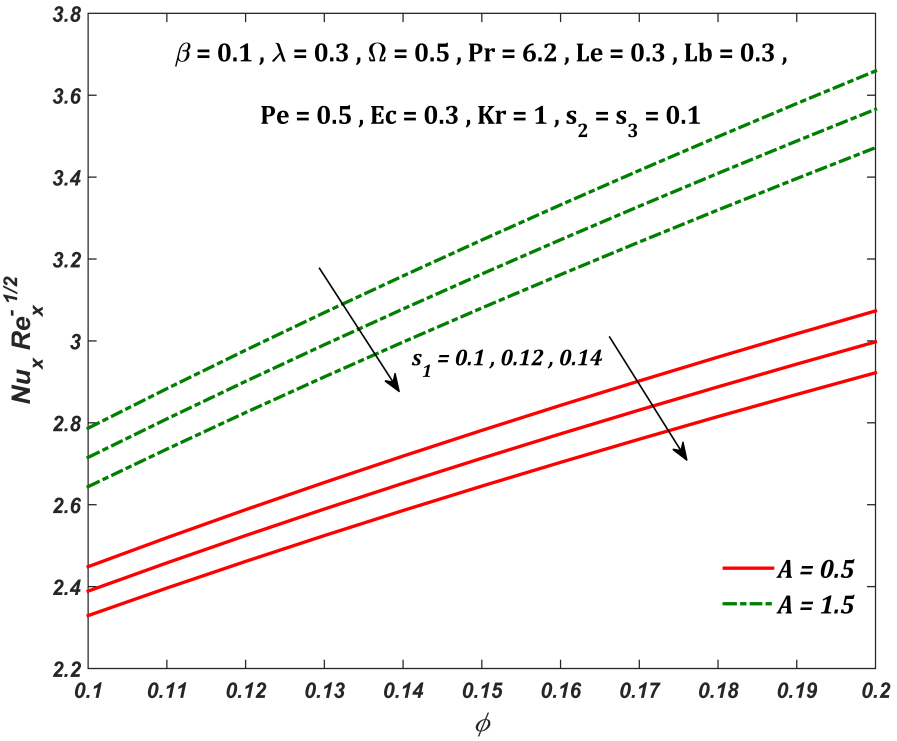

Figure 3.18: Parallel effect of ϕ & s_1 on $Nu_x Re_x^{-1/2}$

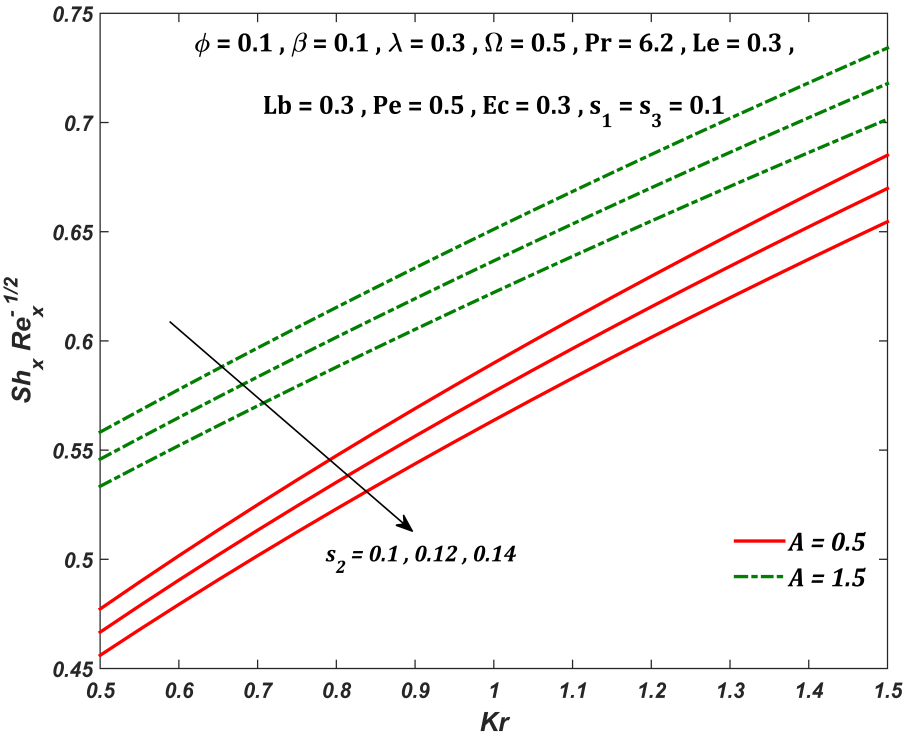

Figure 3.19: Parallel effect of Kr & s_2 on $Sh_x Re_x^{-1/2}$

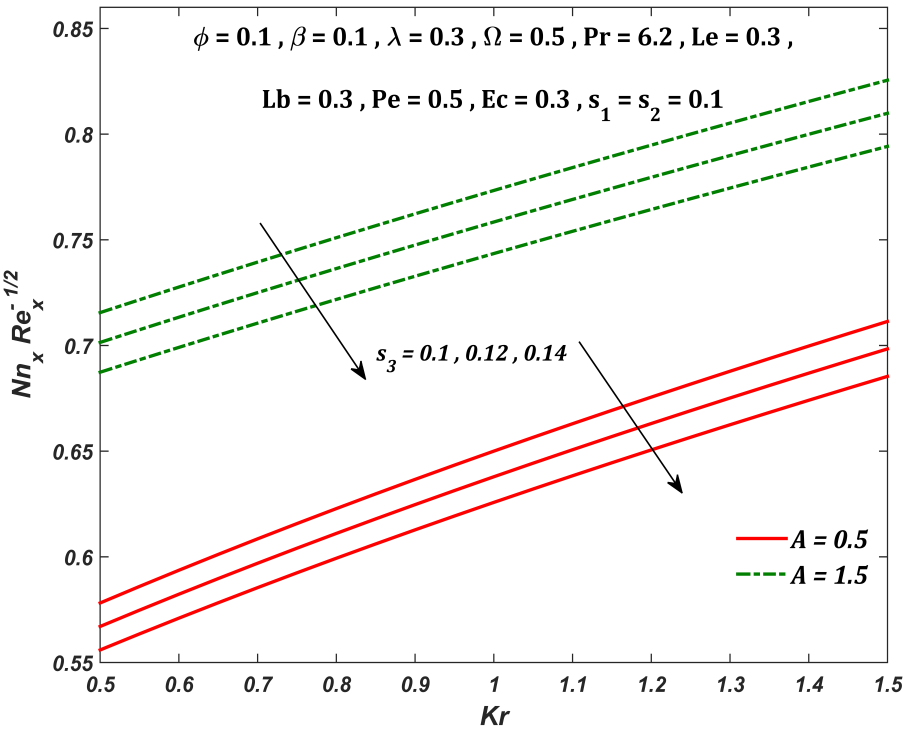

Figure 3.20: Parallel effect of Kr & s_3 on $Nn_x Re_x^{-1/2}$

3.5 Conclusion

The key points noted from the study are:

- The nanomaterial velocity is directly proportional to the magnetic parameter for $A = 0.5$ and inversely proportional when $A = 1.5$.
- Drag coefficient (when $A = 0.5$) ascends with magnetic parameter and descends with nanoparticle volume fraction. However, the results are reversed when $A = 1.5$.
- Eckert number and nanoparticle volume fraction exhibit a constructive effect on the temperature profile.
- Heat transfer is elevated due to nanoparticle volume fraction and lowered with Eckert number and thermal stratification parameter.
- Chemical reaction parameter has a destructive effect on concentration profile.
- Chemical reaction parameter promotes and solutal stratification demotes mass transfer.
- A decline in microorganism, concentration and temperature profiles is observed due to ascending motile density, solutal, thermal stratification parameters, respectively.
- Microorganism density number lowers with motile density stratification parameter.

Appendix I: Non-dimensional qunatities

$A = \frac{a}{c}$	Stretching parameter
$\beta = \frac{\mu_e}{4\pi\rho_f}\left(\frac{H_0}{c}\right)^2$	Magnetic parameter
$\lambda = \frac{1}{4\pi\mu_e\sigma_f\vartheta_f}$	Reciprocal of magnetic Prandtl number
$Pr = \frac{(\mu C_p)_f}{k_f} = \frac{\vartheta_f}{\alpha_f}$	Prandtl number
$Kr = \frac{k_r}{c}$	Chemical reaction parameter
$Ec = \frac{(cx)^2}{(C_p)_f (T_w - T_0)}$	Eckert number
$Le = \frac{\vartheta_f}{D_B}$	Lewis number
$Lb = \frac{\vartheta_f}{D_m}$	Bioconvection Lewis number
$Pe = \frac{bW_c}{D_m}$	Bioconvection Peclet number
$\Omega = \frac{N_\infty}{N_w - N_0}$	Microorganism concentration difference parameter
$s_1 = \frac{\delta_2}{\delta_1}$	Thermal stratification parameter
$s_2 = \frac{\epsilon_2}{\epsilon_1}$	Solutal stratification parameter
$s_3 = \frac{\xi_2}{\xi_1}$	Motile density stratification parameter

Appendix II: Nomenclature

a, c	Dimensional constants	W_c	Maximum cell swimming speed
u, v	Velocity components	H_0	Uniform magnetic field at infinity
Nn_x	Local motile density	T_∞	Ambient fluid temperature
T_0	Reference temperature	N_∞	Ambient microbial concentration
C	Fluid concentration	C_0	Reference nanoparticle concentration
T	Fluid temperature	N_0	Reference microbial concentration
x, y	Cartesian coordinates	N_w	Microbial concentration near wall
b	Chemotaxis constant	C_w	Nanoparticle concentration near wall
T_w	Wall fluid temperature	C_∞	Ambient nanoparticle concentration
C_p	Specific heat	Cf_x	Local drag coefficient
k_r	Reaction rate constant	Nu_x	Local Nusselt number
Sh_x	Local Sherwood number	N	Microorganism concentration
σ	Electrical conductivity	H_e	Magnetic field at free stream
ζ	Dimensionless variable	D_B	Chemical molecular diffusivity
ϑ	Kinematic viscosity	D_m	Microorganism diffusion coefficient
k	Thermal conductivity	Ω	Microorganism concentration difference
μ_e	Magnetic permeability		parameter
ρ	Fluid density	λ	Reciprocal of magnetic Prandtl number
β	Magnetic parameter	ϕ	Nanoparticle volume fraction
α_m	Magnetic diffusivity	α	Thermal diffusivity